Analytica Chimica Acta 1087 (2019) 113–120

Contents lists available at ScienceDirect

Analytica Chimica Acta

journal homepage: www.elsevier.com/locate/aca

# Detachable nanoladders: A new method for signal identification and their application in the detection of ochratoxin A (OTA)

Xiangli Shao [a, b], Longjiao Zhu [b], Yuxiang Feng [b], Yangzi Zhang [b], Yunbo Luo [a, b], Kunlun Huang [a, b, c], Wentao Xu [a, b, c, *]

[a] Beijing Advanced Innovation Center for Food Nutrition and Human Health, College of Food Science and Nutritional Engineering, China Agricultural University, Beijing, 100083, China
[b] Key Laboratory of Safety Assessment of Genetically Modified Organism (Food Safety), College of Food Science and Nutritional Engineering, China Agricultural University, Beijing, 100083, China
[c] Beijing Laboratory for Food Quality and Safety, College of Food Science and Nutritional Engineering, China Agricultural University, Beijing, 100083, China

## HIGHLIGHTS

- A highly sensitive fluorescence biosensor was developed based on OTA-induced detachable nanoladders and GO.
- It integrates the advantages of aptameric recognition of the target and the selective quenching effects provided by GO.
- The presented method achieved great improvements by simply adding two mismatched bases to probes.
- This pioneering biosensor is sensitive, specific, rapid, enzyme-free and cost-effective and can be applied in red wine samples.

## GRAPHICAL ABSTRACT

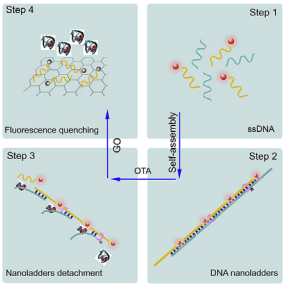


## ARTICLE INFO

*Article history:*
Received 2 January 2019
Received in revised form
9 July 2019
Accepted 25 August 2019
Available online 27 August 2019

*Keywords:*
Detachable nanoladders
Graphene oxide
Aptamer
OTA
Fluorescence biosensor

## ABSTRACT

A highly sensitive fluorescence turn-off biosensor for the detection of ochratoxin A (OTA) was developed based on graphene oxide (GO) and an aptamer-induced detachable nanoladders. In this assay, two types of ssDNA (H1 and H2) were involved in the assembly of the DNA nanoladders, in which H1 was labeled with fluorophore, and H2 was the OTA binding aptamer. Self-assembly of the DNA nanoladders with the addition of GO weakened its adsorption and the fluorescence intensity remained strong. In the presence of OTA, the aptamer was specifically recognized and an aptamer-OTA complex was formed, leading to the detached of DNA nanoladders. With the addition of GO, the released H1 was adsorbed on the GO surface, thus efficiently quenching the fluorescence signal (turning off). The detection limit of OTA in this assay was 4.59 nM. To improve the sensitivity of this strategy, we creatively developed an alternative strategy to replace the sturdy nanoladders with frail nanoladders. More precisely, the sequences of H1 had mismatched bases, which, when hybridized with H2 could be used to create long non-perfect complementary nanoladders. For the mismatched bases-based frail nanoladders, it was easier for OTA to bind its aptamer sequence, thus enabling a more thorough and faster detachment of the nanoladders, along with a greater degree of fluorescence quenching. The detection limit for OTA was estimated to be 0.1 nM. The

* Corresponding author. Beijing Advanced Innovation Center for Food Nutrition and Human Health, College of Food Science and Nutritional Engineering, China Agricultural University, Beijing, 100083, China.
*E-mail address:* xuwentao@cau.edu.cn (W. Xu).

https://doi.org/10.1016/j.aca.2019.08.057

biosensors we developed were sensitive, specific, enzyme-free, cost-effective and can be applied in red wine samples spiked with known concentration of OTA.



## 1. Introduction

Innovative nanomaterials, such as carbon nanostructures, DNA nanostructures and metal nanoparticles, have enabled biofunctionalization with physical and chemical effects [1–3]. These nanomaterials can be used as carriers or tracers [4], electronic conductors [5], and optical emitters [6] to develop stabilized recognition probes and amplified detection signals. The nanomaterials-based biosensor offers new tools for the selective, rapid and cost-effective detection of a wide variety of targets in food safety, both clinical and environmental [7].

Graphene is a flat, two-dimensional, single-layered, and honeycomb-shaped carbon nanomaterial with extraordinary electronic, optical, and surface properties [8,9]. To improve its solubility in water, graphene is oxidized to graphene oxide (GO) [9]. The large surface of GO, which contains several functional groups and domains, makes it an ideal platform for GO–nucleic acid interactions. GO is known to preferentially interact with ssDNA over dsDNA on its surface [10]. The exposed aromatic rings holding $sp^2$ electrons have been suggested to contribute to the π-π stacking between ssDNA and aromatic groups of GO [11]. However, when ssDNA hybridizes with its complementary DNA to form dsDNA, the π-π stacking between the aromatic groups of dsDNA and GO is significantly weakened, because of the inadequate $sp^2$ electrons available to the dsDNA aromatic groups. This reliance on the interaction between GO and DNA, has greatly motivated the development of GO-based fluorescence resonance energy transfer (FRET) biosensors. The critical effect of FRET is that it allows GO to quench the fluorescence near its surface [12,13]. Compared to organic quenchers, GO has shown a greater quenching efficiency than a variety of fluorophores, with advantages such as low background and high signal-to-noise ratio, amongst others, derived from the nanomaterial itself [14]. These advantages have encouraged penetrating research of GO and its wide applications for biosensors [15], drug-delivery [16], and live imaging [17].

DNA nanostructures are nanoscale molecular structures constructed primarily from synthetic DNA [18,19], and commonly formed by self-assembly of DNA driven by entropy [20]. Compared with GO and other nanomaterials, DNA nanostructures have some unique advantages, like their ease of design and the predictability of their geometric structures [21,22]. With the aid of computer design and simulation, diverse engineered DNA nanostructures have been fabricated, such as DNA tile nanostructures, DNA origami and brick nanostructures, three-dimensional DNA nanostructures, DNA machines, and DNA supramolecular nanostructures [23]. Nanoladders are essentially DNA sandwich structures which are a simple DNA nanostructure. The preparation of the DNA nanoladder is a simple and efficient process, generally performed at a constant temperature and without enzymes. A typical supersandwich usually involves two types of ssDNA with alternating units to produce a large quantity of long dsDNA nanostructures. DNA nanostructures have various capabilities, such as their use as templates for the further assembly of other nanomaterials, and the sensitive molecular detection and amplification of molecular recognition events [24]. DNA nanostructures are equipped to detect targets beyond nucleic acids, including small molecules, proteins and cells, which makes them highly demanded and one of the most interesting subjects in the field of biosensors. Although much progress has been achieved in specific nucleic acid detection based on DNA nanostructures, there are still numerous challenges in detecting non-nucleic acid targets.

Aptamers are selected single-strand oligonucleotides (DNA or RNA) isolated from random-sequence libraries by an in vitro election process. They boast high specificity to a variety of targets. By using aptamers as probes, we can extend the targeting field of GO-based biosensors from DNA to ions, small molecules, and proteins [25]. Furthermore, using aptamers as a type of probe fabricated by DNA nanoladders, the detachment of the preformed DNA nanoladders can be applied in the detection of specific non-nucleic acid targets.

Ochratoxin A (OTA) is a fungal-derived food toxin which can cause a number of acute and chronic toxic effects to humans and animals [26]. In previous research, we have developed a biosensor based on DNA nanoladders supported by T–Hg (II)–T and were used for Hg (II) trapping and signal translation [27]. In this study, a simple DNA nanostructure (DNA nanoladder) was introduced to recognize OTA. DNA nanoladders contained multiple OTA-binding sites and fluorescence-labeled probes on each of its long concatemers. Self-assembly of the DNA nanoladders with the addition of GO weakened its adsorption and the fluorescence intensity remained strong. However, the presence of OTA induced detachment of the nanoladders and fluorescence-labeled probes were released, adsorbed on the GO surface, and efficiently quenched (turned off). In this approach, a reliable detection limit of 4.59 nM for OTA was achieved. To further improve the sensitivity and accuracy of this biosensor, a novel fluorescence turn-off biosensor based on mismatching nanoladders was developed. With mismatched bases, the nanoladders were frail and easier to detach. Using this method, the detection limit of OTA was successfully decreased to 0.1 nM. In the future, this optical biosensor can be used for the detection of disease-related small molecular targets, and it further offers numerous other practical applications in biotechnology and life science.

## 2. Materials and methods

### 2.1. Chemical reagent

The GO aqueous solution was purchased from Nanjing XFNANO Materials Tech Co., Ltd. Ochratoxin A (OTA) was extracted by our laboratory, and the results of the high-performance liquid chromatography (HPLC) measured its concentration at 17.686 mM. All of the nucleic acids used in this work were synthesized by KareBay Biochem Inc., and lyophilized nucleic acids were dissolved in distilled water before use. The DNA sequences are listed in Table S1 and Table S3. All other reagents were of analytical grade and used without further purification or modification. DNA markers were purchased from Tiangen Biotechnology Co., Ltd. The ultrapure water used throughout was prepared via the Millipore Milli-XQ system (Millipore).

### 2.2. DNA sequences for nanoladders

All the synthetic DNA sequences, as listed in Table S1, were

commercially synthesized at KareBay Biochem Inc. The 5' of H1 were labeled with a ROX fluorophore, while those of H2 were the aptamers of OTA. Alternating units of H1 and H2 were successively hybridized to each other, resulting in a long set of DNA nanoladderes. The complementary section between H1 and H2 is highlighted in the same color in Table S1.

### 2.3. Apparatus

The agarose gel electrophoresis images were visualized in a BioDoc-It Imaging System (UVP, USA). The circular dichroisms (CD) were detected using a Chirascan™-plus CD Spectrometer (Applied Photophysics, UK). The fluorescence images were acquired on a Nikon Eclipse Ti-E inverted microscope (Nikon, UK). The fluorescence intensities were monitored by a CFX96 real-time PCR thermocycler (Bio-Rad) in the ROX channel at 20 °C. The fluorescence spectra were collected using a Cary Eclipse Fluorescence Spectrophotometer (Agilent Technologies, Inc.).

### 2.4. Gel electrophoresis

First, 1 μM H1 was incubated with 1 μM H2 in a 10 mM Tris-HCl buffer containing 1 mM $MgCl_2 \cdot 6H_2O$ (pH 7.4) for 30 min at 37 °C to produce the nanoladders. Subsequently, the formed nanoladders were the detached in the presence of 100 μM OTA at 37 °C for 2 h. Finally, the OTA-induced detachment product was analyzed using a 2% agarose gel. 1 g of agarose was adding to 50 mL of 1 × TAE buffer (40 mM tris acetate, 2.0 mM $Na_2EDTA$, pH 8.0), and then mixed with 0.5 μL ethidium bromide (EB) (Tiangen Biotechnology Co., Ltd.) to dye the gel. The agarose gel with samples was run at 130 V for 25 min in 1 × TAE buffer and then photographed by a BioDoc-It Imaging System (CA, USA).

### 2.5. Fluorescence turn-off biosensor for the detection of OTA

First, 150 nM ROX-labeled H1 was incubated with 150 nM H2 in a 10 mM Tris-HCl buffer containing 1 mM $MgCl_2 \cdot 6H_2O$ (pH 7.4) at 37 °C for 30 min to form the nanoladders. Different concentrations of OTA were then introduced into the nanoladders at 37 °C for 2 h. The OTA was observed to recognize the aptamer probes of the nanoladders and inducing the detachment of the nanoladders. Next, 15 mg/L GO was added by incubation with the assembly (negative control group) and detachment (test group) systems at room temperature for 5 min. Finally, the fluorescence intensities were monitored by means of a CFX96 real-time PCR thermocycler in the ROX channel at 20 °C. The fluorescence spectra were collected using a Cary Eclipse Fluorescence Spectrophotometer. The excitation wavelength was determined to be 587 nm and the emission wavelength was monitored from 595 nm to 680 nm.

## 3. Results and discussion

### 3.1. The principle of the fluorescence turn-off biosensor

Two types of ssDNA (H1 and H2) were involved in the production of a large quantity of long dsDNA nanostructures with periodical units, termed as DNA nanoladders (Scheme 1a). In the DNA nanoladders, H1 was labeled with a ROX fluorophore, and H2 was the OTA binding aptamer. Self-assembly of the DNA nanoladders with the addition of GO weakened its adsorption and the fluorescence intensity remained strong. In the presence of OTA, H2 associated with OTA formed an aptamer-OTA complex, and the H1 was thus released. With the addition of GO, the free H1 was adsorbed on the GO surface, and their fluorescence was efficiently quenched (turned off) (Scheme 1b).

### 3.2. Feasibility of the OTA-induced detachable nanoladders

Gel electrophoresis was performed to confirm the formation and detachment of the nanoladders (Fig. 1a). First, H1 was mixed with H2 in the environmental solution. A ladder of different lengths of the nanoladders, with the maximum length being ~750 base pairs, was observed in lane 4, thus suggesting the formation of the nanoladders. After the addition of OTA, after which only ~100 base pairs were observed in lane 5, which might be the dimer of H1 (lane 2), thus suggesting that the nanoladders were successfully detachment in the solution.

CD analysis provided further confirmation of the feasibility of the disassembly of the nanoladders. As shown in Fig. 1b, CD spectra of the nanoladders were notably different with and without OTA. The OTA caused a clear right shift in the elliptic around 260 nm and 290 nm. The CD spectrum of H1+H2 had a greatly enhanced positive band at 290 nm and a greatly enhanced negative band at about 260 nm. It has to be noted that there was a new peak in the negative elliptic minimum around 235 nm upon addition of OTA. These results indicated that the conformation transformation of the nanoladders was changed upon the OTA's binding.

### 3.3. Effect of buffers, probes and GO on the quenching efficiency

Salt ions are an important factor for the highly stable secondary structures of DNA sequences in biosensors. In this study, five types of buffer solution were employed (Table S2). The factor of quenching efficiency was defined as

$$\text{Quenching efficiency} = \frac{F0 - F}{F0}$$

where F0 and F represent the fluorescence intensity in the solution, with and without GO, respectively.

The quenching efficiency values of H1, the nanoladders, and the OTA-induced detachment of the nanoladders system were determined. As shown in Fig. 2a, GO was effective in quenching the fluorescence signal of H1 in buffer E (~96%). With the addition of GO, the fluorescence of the nanoladder was mostly retained (~50%), while the fluorescence of the OTA-induced detachment of nanoladder was mostly quenched (~88%). Tris-HCl buffer (buffer E) was remarkably effective than other four phosphate buffers (buffer A, buffer B, buffer C and buffer D) in this biosensor. It was likely that the nanoladders were easier to detach in Tris-HCl buffer than in phosphate buffers. Compared with the four phosphate buffers, the types and concentration of ions determined the adsorption capacity of DNA with GO. For example, the components of buffer B were identical to those in buffer A, with the exception of the divalent ions ($Mg^{2+}$). Notably, ~87% fluorescence quenching of the ROX-H1 was observed in buffer B, while the quenching efficiency appeared to be much lower in buffer A (~57%). This is probably because the divalent metal ions were much more effective in screening charges and acting as a bridge to connect two negatively charged molecules in comparison to the monovalent ones [28,29]. Finally, buffer E (10 mM Tris-HCl, 1.0 mM $MgCl_2$) was effective in the OTA assays.

Furthermore, the concentration of GO and the amplification efficiency of the nanoladders were crucial to the quenching efficiency of nanoladders and the detachment of nanoladders. So the concentration of H1 and H2 and GO used in this work were explored to achieve the highest quenching efficiency. As shown in Fig. 2b, when the concentration of H1 and H2 higher than 50 nM, the Δquenching efficiency of H1 and nanoladders decreased obviously as the increase of GO concentration in the range of 15–35 mg/L Δquenching efficiency was calculated as

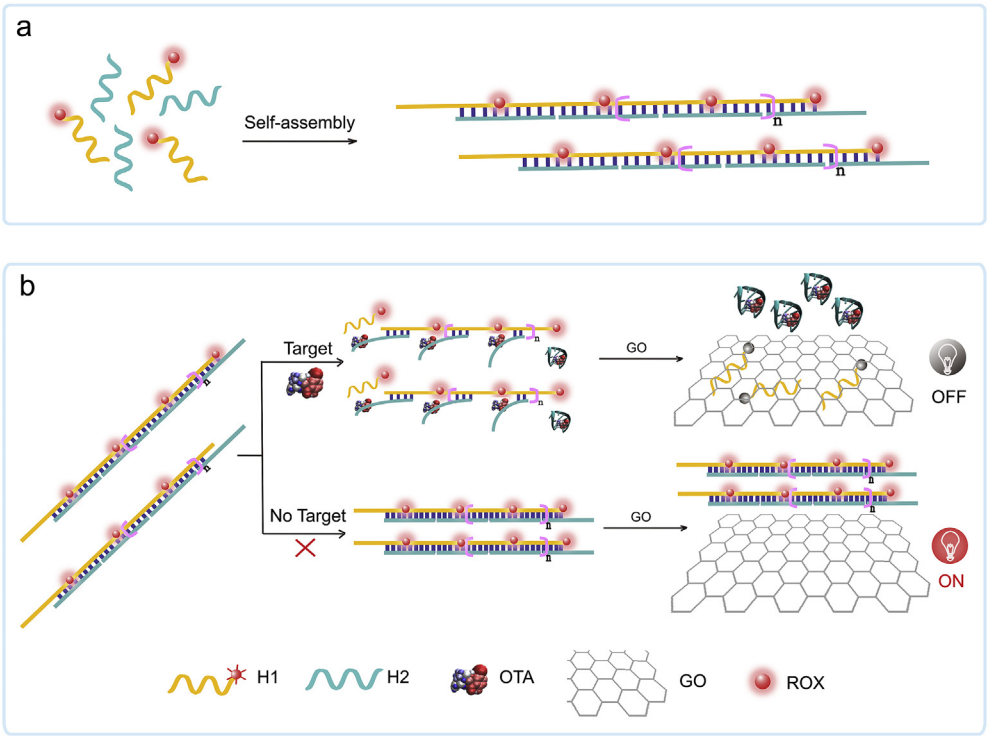


**Scheme 1.** Illustration of the biosensor based on GO and detachable nanoladders for OTA detection. a) The assembly of DNA nanoladders. b) OTA induced detachment.

$$\Delta\textbf{Quenching efficiency} = \frac{\boldsymbol{F}0H1 - \boldsymbol{F}H1}{\boldsymbol{F}0H1} - \frac{\boldsymbol{F}0(H1+H2) - \boldsymbol{F}(H1+H2)}{\boldsymbol{F}0(H1+H2)}$$

where F0 and F represented the fluorescence intensity in the solution with and without GO, respectively.

ΔQuenching efficiency was defined as the D-value of quenching efficiency between H1+H2 (dsDNA) and H1 (ssDNA). The larger the Δquenching efficiency, the greater performance of this sensor. When the concentration of GO was higher than 21 mg/L, the quenching efficiency was positively related to the concentration of H1 and H2. With increasing concentrations of H1/H2, the quenching efficiency increased significantly. The results prove that GO at low concentration (15 mg/L) possesses the best quenching efficiency, of ~50% at the concentration of 150 nM H1 and H2. It is obvious that the Δquenching efficiency at the concentration of 15 mg/L GO and 150 nM H1 and H2 was the highest. Therefore, 150 nM H1 and H2, with 15 mg/L GO, were employed for analytical purposes in this work.

### 3.4. Optimization of the incubation time of nanoladders with OTA

In order to obtain good linearity in a relatively short period of time, the incubation time of the nanoladders with OTA was optimized. The fluorescence of the nanoladders was quenched effectively (~95%) after incubation of only 5 min with OTA (Fig. 3a).

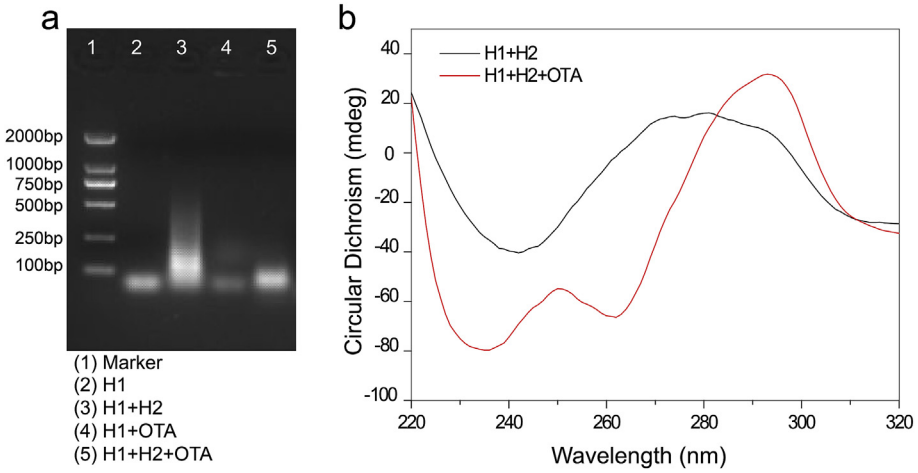


**Fig. 1.** Characterization of the detachment of nanoladders in solution. a) Gel electrophoresis images. b) Circular dichroism spectra (CD).

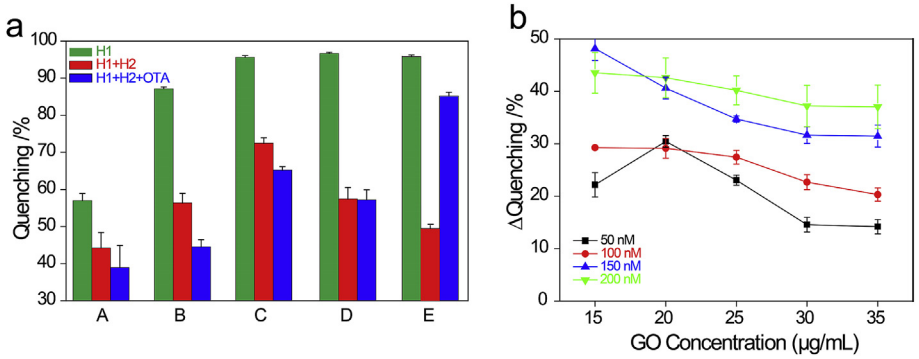


**Fig. 2.** Effect of buffers, probes and GO on the quenching efficiency. a) Effect of buffers. The concentrations of GO and DNA were 15 mg/L and 150 nM, respectively. b) Effect of the concentration of probes and GO.

However, the fluorescence signal of the nanoladders incubating with OTA under different time limitations before the addition of GO (Fig. 3b) was remarkably self-quenched in 5 min and then recovered in 2 h. This phenomenon may be related to the distance between the fluorophore and the OTA. We assumed that the OTA-induced disassembly was probably a two-step process for the following reason: Firstly, the OTA recognized its aptamer in the nanoladders and, owing its aromatic rings, the FRET between the OTA and ROX quickly quenched the fluorescence within a few minutes. Secondly, upon the OTA's association with its aptamers to form the aptamer-OTA complex, triggering the increase in the fluorescence signal during the incubation time. After 2 h, the fluorescence had recovered, which suggests that the disassembly of the nanoladders had reached a dynamic balance. Notably, however, the fluorescence signal decreased again after 20 h, possibly due to its lengthy exposure to photobleaching. The effectively OTA-induced detachment of the nanoladder was confirmed by gel electrophoresis (Fig. S2), which has shown that a period of 2 h was employed as the optimal detachment time in this work to ensure the precision of the experimental results.

### 3.5. Feasibility of the fluorescence turn-off biosensor

Fig. 4 depicts the fluorescence emission spectra of the biosensor in response to OTA. According to Fig. 4a, the fluorescence signal produced by H1 (black curve) was high, however, significant fluorescence quenching was observed after the addition of GO (red curve). By contrast, when H1 was hybridized with H2, the fluorescence was mostly retained with the addition of GO (blue curve). However, in the presence of OTA, significant fluorescence quenching was observed after GO was added (cyan curve), thus indicating that the OTA was specifically recognized with the aptamer, which caused the detachment of nanoladders. The intuitive results, displayed in Fig. 4b, confirmed that in the presence of GO, the fluorescence quenching of H1 was approximately 96%, and the fluorescence quenching of the nanoladders was approximately 50%. The binding affinity of dsDNA to GO could be attributed to partial deformation of the double helix on GO and the hydrogen-bond formation between oxygenous groups of GO and DNA bases [30]. The OTA was again observed to promote the fluorescence quenching effectively, by approximately 88%.

### 3.6. Analytical performance of fluorescence OTA assay

Examination of the relationship between fluorescence quenching efficiency and the amount of OTA revealed a linear relationship in the concentration range of 50 nM–80 nM, as shown in Fig. 5a and represented by $y = 0.86x + 20.129$ ($R^2 = 0.9874$). The detection limit for OTA was estimated to be 4.59 nM (LOD = 3σ/S, where σ is the standard deviation for the blank, S is the slope of calibration curve). Notably, this biosensor showed higher selectivity toward the target (OTA) than the other four types of mycotoxins, namely T-2, DOM, AMF1, and AFB1 (Fig. 5b). The high specificity can be attributed to the target-specific change in the detachable nanoladders.

### 3.7. Feasibility of the more detachable nanoladders

To further improve the sensitivity and accuracy of this biosensor, we first created a frail detachable nanoladders. It is known that the

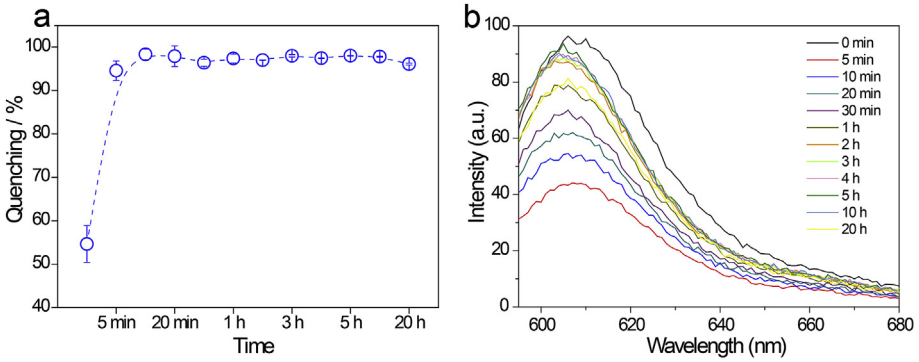


**Fig. 3.** Effect of the incubation time of nanoladders with OTA. a) The quenching efficiency of the nanoladders with OTA in different incubation times. b) Before adding GO, the fluorescence emission spectra of the nanoladders with OTA under different incubation times.

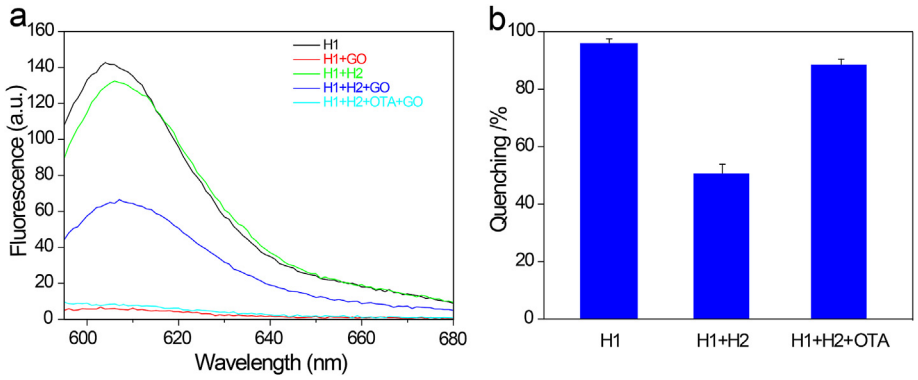


**Fig. 4.** a) The fluorescence emission spectra of the fluorescence turn-off biosensor. b) Percentage of fluorescence quenching in OTA assay system.

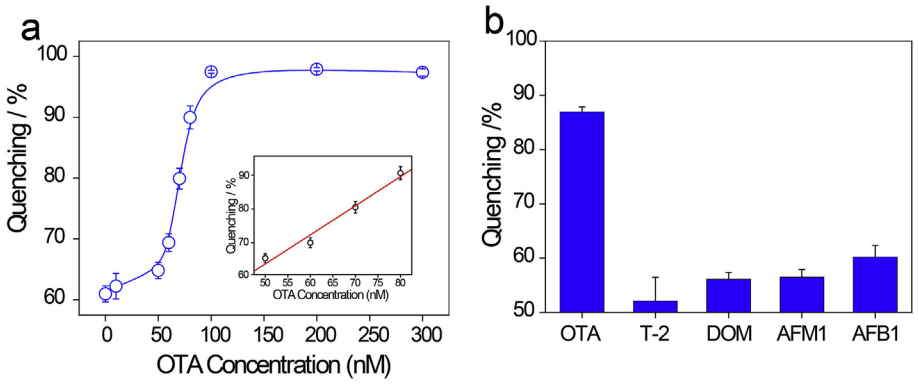


**Fig. 5.** The sensitivity and selectivity of the biosensor for OTA detection. Dose-response curves. a) The concentrations of OTA were 0 nM, 10 nM, 50 nM, 60 nM, 70 nM, 80 nM, 100 nM, 200 nM and 300 nM, respectively. b) Selectivity of the fluorescence assay for OTA over T-2, DOM, AFM1 and AFB1 (all at a concentration of 10 μM).

$T_m$ of a duplex depends on the sequence on the DNA strand in the duplex [31]. Therefore, the mismatched bases were used to decrease the $T_m$ of the hybrid formed frail nanoladders. The duplex structure of the perfectly matched nanoladders was stable and cannot be easily disassembled by OTA due to its high $T_m$. For the mismatched bases-based frail nanoladders with low $T_m$, it was easier for the OTA to bind its aptamer sequence, thus enabling a more thorough and faster detachment of the nanoladders.

As a result, more fluorescence quenching was observed, as was schematically shown in Fig. 6a. The sequences of H1 with a different number of mismatched bases was listed in Table S3. The formation of frail nanoladders were confirmed by gel electrophoresis (Fig. S2). The background signal depended on the amplification efficiency of the frail nanoladders, the higher the amplification efficiency, the lower the background. As shown in Fig. S2, the amplification efficiency of the frail nanoladders was too low based on H2-6 and H2-10, while the amplification efficiency was high based on H2-2. The quenching effect was decided by the $T_m$ of the frail nanoladders. The improvement of the mismatched bases resulted in the decreased of the $T_m$ of the frail nanoladders. On the premise of low background, the lower $T_m$, the higher quenching effect. To balance the background and quenching efficiency, H2-2 based frail nanoladders were chose to fabricate the novel biosensor. The formed frail nanoladders were incubated with OTA under different reaction times (Fig. S3). Compared to the perfectly matched group, the time variations of the OTA-induced detachable of the frail nanoladders were more obvious (lane 10–17). The incubation time of the frail nanoladders with OTA was optimized. As shown in Fig. S4, the OTA-induced disassembly process of the frail nanoladders was similar to nanoladders incubating with OTA under different time limitations. A period of 1 h was employed as the optimal detachment time of the frail nanoladders, which was shorter than the incubation time of nanoladders with OTA. The effecct of salt ions of the frail nanoladders was optimized. As shown in Fig. S5, Tris-HCl buffer (buffer E) was also remarkably effective than other four phosphate buffers (buffer A-D) in the biosensor based on frail nanoladders.

As expected, more fluorescence quenching was observed in the two-base mismatched nanoladders (~85%) than the perfectly matched nanoladders (~60%), when the concentration of OTA was 10 nM (Fig. 6b). The fluorescence emission spectra further verified the feasibility of the novel biosensor based on a frail nanoladder (Fig. 6c). The more intuitive results shown in Fig. S4 provided an effective comparison. Further elevating with variations of OTA concentration from 0.1 nM to 100 nM. The amount of OTA revealed a linear relationship in the concentration range of 1 nM–10 nM, represented by $y = 2.91x + 55.33$ ($R^2 = 0.9788$), as shown in Fig. 6d. The detection limit for OTA was estimated to be 0.1 nM (LOD = 3σ/S, where σ is the standard deviation for the blank, S is the slope of calibration curve), which is lower than those of the sensors previously reported [32–34].

### 3.8. Application in wine samples

To confirm if our method can be applied in food samples, three different concentrations of OTA spiked into wine samples were monitored. As shown in Table 1, the recovery ratio of spiked wine samples by our method was 87–114%, which enabled the range required by Directive 98/53/EC. In addition, this sensitivity is lower than the standard residue levels regulated by the European Union (EU) regulations. (2 μg/kg) [35], suggesting the strategy developed

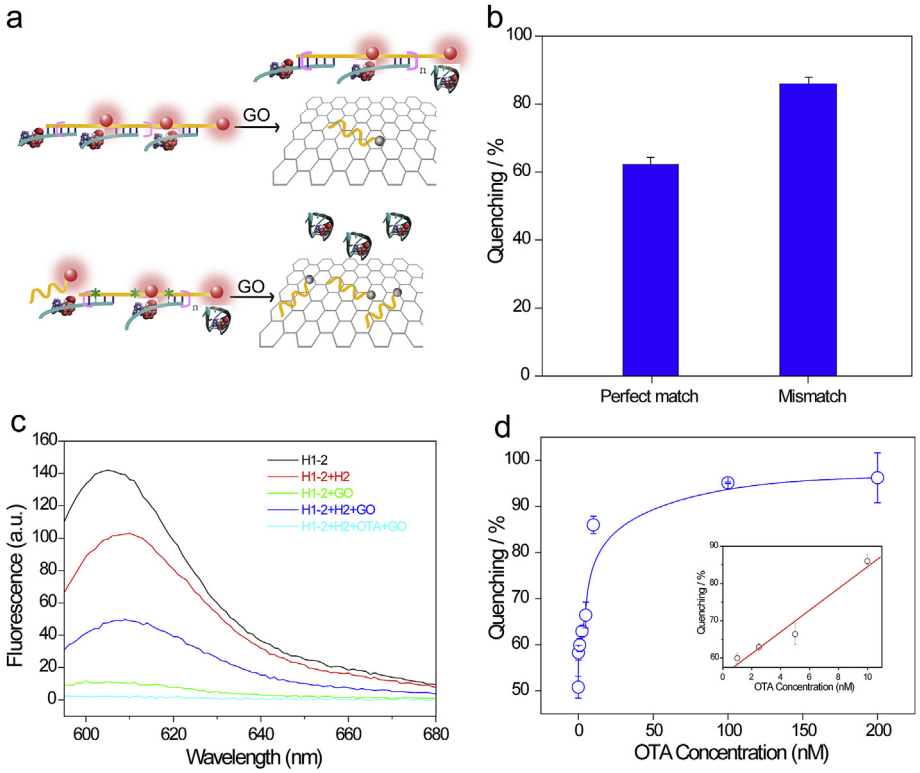


**Fig. 6.** The feasibility and sensitivity of the novel biosensor based on frail detachable nanoladders and GO. a) Scheme showing the OTA-induced detachment of mismatched nanoladders (bottom) are easier than perfect matched nanoladders (top), green * represent the mismatch sites. b) The comparison of fluorescence quenching. c) The fluorescence emission spectra of the novel biosensor. d) Dose-response curves. The concentrations of OTA were 0 nM, 0.1 nM, 1 nM, 2.5 nM, 5 nM, 10 nM, 100 nM, and 200 nM, respectively. (For interpretation of the references to color in this figure legend, the reader is referred to the Web version of this article.)

**Table 1**
Recovery of OTA from wine samples by the fluorescent method (n = 3).

| OTA spiked (nM) | OTA detected (nM) | R.S.D. (%) | Recovery (%) |
|---|---|---|---|
| 1 | 1.14 | 6.15 | 114 |
| 2 | 1.74 | 10.11 | 87 |
| 5 | 5.36 | 5.94 | 107.2 |

can be reliable as a quantitative method for OTA detection in real samples.

## 4. Conclusion

In conclusion, a new method for detection of OTA was presented, based on GO and the modulation of nanoladders, with an OTA detection limit of 4.59 nM. To improve the sensitivity of this strategy, a novel method based on frail detachable nanoladders was developed, with a detection limit of 0.1 nM. The biosensor has excellent specificity, which combines aptameric recognition of the target that induced the conformation change of frail detachable nanoladders with the selective quenching effects of GO. The biosensor has been applied for monitoring OTA in red wine samples. Besides, this biosensor offers great potential for use with other molecular analytes, and even disease-related molecular targets, as well as other practical applications in biotechnology and life science in the future.

## Declaration of competing interest

The authors declare that they have no known competing financial interests or personal relationships that could have appeared to influence the work reported in this paper

## Acknowledgment

This work was financially supported by the National GMO Cultivation Major Project of New Varieties (Grant No. 2018ZX08012-001) and National Natural Science Foundation of China (Grant No. 31671922).

## Appendix A. Supplementary data

Supplementary data to this article can be found online at https://doi.org/10.1016/j.aca.2019.08.057.

## References

[1] M. Rejzek, V.S. Kannathasan, C. Wing, A. Preston, E.L. Westman, J.S. Lam, J.H. Naismith, D.J. Maskell, R.A. Field, Chemical synthesis of UDP-Glc-2, 3-diNAcA, A key intermediate in cell surface polysaccharide biosynthesis in the human respiratory pathogens B. pertussis and P. aeruginosa, Org. Biomol. Chem. 7 (2009) 1203–1210.
[2] W. Zhao, W. Chiuman, J.C. Lam, S.A. McManus, W. Chen, Y. Cui, R. Pelton, M.A. Brook, Y. Li, DNA aptamer folding on gold nanoparticles: from colloid chemistry to biosensors, J. Am. Chem. Soc. 130 (2008) 3610–3618.
[3] R. Freeman, X. Liu, I. Willner, Chemiluminescent and chemiluminescence resonance energy transfer (CRET) detection of DNA, metal ions, and aptamer–substrate complexes using hemin/G-quadruplexes and CdSe/ZnS quantum dots, J. Am. Chem. Soc. 133 (2011) 11597–11604.
[4] M. Wanunu, T. Dadosh, V. Ray, J. Jin, L. McReynolds, M. Drndić, Rapid electronic detection of probe-specific microRNAs using thin nanopore sensors, Nat. Nanotechnol. 5 (2010) 807.
[5] Z. Wu, Z. Zhen, J.-H. Jiang, G.-L. Shen, R.-Q. Yu, Terminal protection of small-molecule-linked DNA for sensitive electrochemical detection of protein binding via selective carbon nanotube assembly, J. Am. Chem. Soc. 131 (2009) 12325–12332.
[6] H. Li, L. Rothberg, Colorimetric detection of DNA sequences based on

electrostatic interactions with unmodified gold nanoparticles, Proc. Natl. Acad. Sci. U.S.A. 101 (2004) 14036–14039.
[7] J. Lei, H. Ju, Signal amplification using functional nanomaterials for biosensing, Chem. Soc. Rev. 41 (2012) 2122–2134.
[8] M.J. Allen, V.C. Tung, R.B. Kaner, Honeycomb carbon: a review of graphene, Chem. Rev. 110 (2009) 132–145.
[9] K.S. Novoselov, A.K. Geim, S.V. Morozov, D. Jiang, Y. Zhang, S.V. Dubonos, I.V. Grigorieva, A.A. Firsov, Electric field effect in atomically thin carbon films, Science 306 (2004) 666–669.
[10] C.H. Lu, H.H. Yang, C.L. Zhu, X. Chen, G.N. Chen, A graphene platform for sensing biomolecules, Angew. Chem. Int. Ed. 121 (2009) 4879–4881.
[11] E. Morales-Narváez, A. Merkoçi, Graphene oxide as an optical biosensing platform, Adv. Mater. 24 (2012) 3298–3308.
[12] R. Swathi, K. Sebastian, Resonance energy transfer from a dye molecule to graphene, J. Chem. Phys. 129 (2008) 054703.
[13] P.R. Selvin, The renaissance of fluorescence resonance energy transfer, Nat. Struct. Mol. Biol. 7 (2000) 730.
[14] Z. Tang, H. Wu, J.R. Cort, G.W. Buchko, Y. Zhang, Y. Shao, et al., Constraint of DNA on functionalized graphene improves its biostability and specificity, Small 6 (2010) 1205–1209.
[15] S.K. Krishnan, E. Singh, P. Singh, M. Meyyappan, H.S. Nalwa, A review on graphene-based nanocomposites for electrochemical and fluorescent biosensors, RSC Adv. 9 (2019) 8778–8881.
[16] Y. Wei, F. Zhou, D. Zhang, Q. Chen, D. Xing, A graphene oxide based smart drug delivery system for tumor mitochondria-targeting photodynamic therapy, Nanoscale 8 (2016) 3530–3538.
[17] L. Yang, B. Liu, M. Wang, J. Li, W. Pan, X. Gao, et al., A highly sensitive strategy for fluorescence imaging of microRNA in living cells and in vivo based on graphene oxide-enhanced signal molecules quenching of molecular beacon, ACS Appl. Mater. Interfaces 10 (2018) 6982–6990.
[18] E. Winfree, F. Liu, L.A. Wenzler, N.C. Seeman, Design and self-assembly of two-dimensional DNA crystals, Nature 394 (1998) 539.
[19] P. Rothemund, Assembly and characterization of 8-arm and 12-arm DNA branched junctions, Nature 440 (2006) 297.
[20] D.Y. Zhang, A.J. Turberfield, B. Yurke, E. Winfree, Engineering entropy-driven reactions and networks catalyzed by DNA, Science 318 (2007) 1121–1125.
[21] J. Bath, A.J. Turberfield, DNA nanomachines, Nat. Nanotechnol. 2 (2007) 275.
[22] T.H. LaBean, H. Li, Constructing novel materials with DNA, Nano Today 2 (2007) 26–35.
[23] K.E. Bujold, A. Lacroix, H.F. Sleiman, DNA nanostructures at the interface with biology, Chem 4 (2018) 495–521.
[24] Y. Jiang, N. Liu, W. Guo, F. Xia, L. Jiang, Highly-efficient gating of solid-state nanochannels by DNA supersandwich structure containing ATP aptamers: a nanofluidic IMPLICATION logic device, J. Am. Chem. Soc. 134 (2012) 15395–15401.
[25] A.D. Ellington, J.W. Szostak, In vitro selection of RNA molecules that bind specific ligands, Nature 346 (1990) 818.
[26] A. Lühe, H. Hildebrand, U. Bach, T. Dingermann, H.-J. Ahr, A new approach to studying ochratoxin A (OTA)-induced nephrotoxicity: expression profiling in vivo and in vitro employing cDNA microarrays, Toxicol. Sci. 73 (2003) 315–328.
[27] Y. Feng, X. Shao, K. Huang, J. Tian, X. Mei, Y. Luo, et al., Mercury nanoladders: a new method for DNA amplification, signal identification and their application in the detection of Hg(II) ions, Chem. Commun. 54 (2018) 8036–8039.
[28] B. Liu, Z. Sun, X. Zhang, J. Liu, Mechanisms of DNA sensing on graphene oxide, Anal. Chem. 85 (2013) 7987–7993.
[29] S. Liu, K. Ghosh, M. Muthukumar, Polyelectrolyte solutions with added salt: a simulation study, J. Chem. Phys. 119 (2003) 1813–1823.
[30] L. Tang, H. Chang, Y. Liu, J. Li, Duplex DNA/graphene oxide biointerface: from fundamental understanding to specific enzymatic effects, Adv. Funct. Mater. 22 (2012) 3083–3088.
[31] K.J. Breslauer, R. Frank, H. Blocker, L.A. Marky, Predicting DNA duplex stability from the base sequence, Proc. Natl. Acad. Sci. U.S.A. 83 (1986) 3746–3750.
[32] L. Zhu, X. Shao, Y. Luo, K. Huang, W. Xu, Two-way gold nanoparticle label-free sensing of specific sequence and small molecule targets using switchable concatemers, ACS Chem. Biol. 12 (2017) 1373–1380.
[33] L. Lv, D. Li, R. Liu, C. Cui, Z. Guo, Label-free aptasensor for ochratoxin A detection using SYBR Gold as a probe, Sens. Actuators B Chem. 246 (2017) 647–652.
[34] Y. Zhao, R. Liu, W. Sun, L. Lv, Z. Guo, Ochratoxin A detection platform based on signal amplification by exonuclease III and fluorescence quenching by gold nanoparticles, Sens. Actuators B Chem. 255 (2018) 1640–1645.
[35] L. Liu, L. Xu, S. Suryoprabowo, S. Song, H. Kuang, Development of an immunochromatographic test strip for the detection of ochratoxin A in red wine, Food Agric. Immunol. (2017) 1–11.